

## RESEARCH NOTE FROM COLLABORATION

# Energy resolution and the linearity of the CMS forward quartz fibre calorimeter pre-production-prototype (PPP-I)

A S Ayan<sup>1</sup>, N Akchurin<sup>1,11</sup>, U Akgun<sup>1</sup>, E W Anderson<sup>2</sup>, Z Bagoly<sup>3</sup>,  
G Y Bencze<sup>3</sup>, P Bruecken<sup>1</sup>, G Debreczeni<sup>3</sup>, I Dumanoglu<sup>4</sup>, E Eskut<sup>4</sup>,  
A Fenyvesi<sup>5</sup>, V Gavrillov<sup>6</sup>, A Gribushin<sup>7</sup>, C Hajdu<sup>3</sup>, J Hauptman<sup>2</sup>,  
A Kayis<sup>4</sup>, V Kolosov<sup>6</sup>, S Kuleshov<sup>6</sup>, J P Merlo<sup>1</sup>, M Miller<sup>1</sup>, E McCliment<sup>1</sup>,  
J Molnar<sup>5</sup>, A Nikitin<sup>6</sup>, Y Onel<sup>1</sup>, G Onengut<sup>4</sup>, D Osborne<sup>8</sup>, N Ozdes-Koca<sup>4</sup>,  
V Pikalov<sup>6</sup>, A Polatoz<sup>4</sup>, I Schmidt<sup>1</sup>, M Serin<sup>9</sup>, R Sever<sup>9</sup>, V Stolin<sup>6</sup>,  
A Ulyanov<sup>6</sup>, A Umashev<sup>6</sup>, S Uzunian<sup>6</sup>, G Vesztergombi<sup>3</sup>, D Winn<sup>10</sup>,  
A Yershov<sup>7</sup>, P Zalan<sup>3</sup> and M Zeyrek<sup>9</sup>

<sup>1</sup> University of Iowa, Iowa City, USA

<sup>2</sup> Iowa State University, Ames, USA

<sup>3</sup> KFKI-RMKI, Budapest, Hungary

<sup>4</sup> Cukurova University, Adana, Turkey

<sup>5</sup> ATOMKI, Debrecen, Hungary

<sup>6</sup> ITEP, Moscow, Russia

<sup>7</sup> Nuclear Physics Institute of Moscow State University, Moscow, Russia

<sup>8</sup> Boston University, Boston, USA

<sup>9</sup> Middle East Technical University, Ankara, Turkey

<sup>10</sup> Fairfield University, Fairfield, USA

E-mail: yasar-onel@uiowa.edu

Received 9 April 2004

Published 27 October 2004

Online at [stacks.iop.org/JPhysG/30/N33](http://stacks.iop.org/JPhysG/30/N33)

doi:10.1088/0954-3899/30/12/N01

## Abstract

The first pre-production-prototype (PPP-I) of the quartz fibre calorimeter of the CMS detector has been tested at CERN. The calorimeter consists of quartz fibres embedded in an iron matrix. Results are presented on the energy resolution and on the signal uniformity of the prototype for electrons and pions and the signal uniformity and linearity.

(Some figures in this article are in colour only in the electronic version)

<sup>11</sup> Now at Texas Tech University, Lubbock, USA.

## 1. Introduction

The CMS [1] detector will look for the Higgs and SUSY particles. The HF detector will play an important role in these searches by improving the missing transverse energy measurement and enabling the tagging of the forward jets. A good missing transverse energy measurement is essential to the standard model Higgs search by  $H \rightarrow WW \rightarrow lvjj$  channels. It is also crucial in SUSY Higgs searches for  $H \rightarrow \tau\tau \rightarrow e\mu + E_T^{\text{miss}}$  and  $H \rightarrow \tau\tau \rightarrow lh + E_T^{\text{miss}}$  to make Higgs mass reconstruction possible. For the  $H \rightarrow WW \rightarrow lvjj$  and  $H \rightarrow ZZ \rightarrow lvjj$  channels, two forward jet tagging is also important. These jets are energetic with a longitudinal momentum of  $\langle p_L \rangle \approx 1$  TeV and a transverse momentum of  $m_W$ . They are produced in the pseudo-rapidity region  $2.0 < \eta < 5.0$  which falls into the forward calorimeter (HF) region.

Calorimeters are a crucial part of the CMS detector. The electromagnetic calorimeter will measure the energies of electrons and photons. It is particularly important for the detection of the decay of the Higgs into two photons. Since the mass resolution of this channel depends on the performance of the detector, an energy resolution of  $5\%/\sqrt{E} + 0.5\%$  is required above 100 GeV [2].

The hadronic calorimeters will help measure quark, gluon and neutrino directions and energies by determining the energy and direction of particle jets and missing transverse energy. They will also help determine the identification of electrons, photons and muons in conjunction with the electromagnetic calorimeter and the muon detectors. The pseudo-rapidity range of  $\eta < 3.0$  is covered by the hadron barrel (HB) and hadron end-cap (HE) calorimeters [3]. The central calorimeters require moderate single particle and jet energy resolutions ( $\sim 100\%/\sqrt{E}$  for HB and  $\sim 150\%/\sqrt{E}$  for HE).

To extend the pseudo-rapidity region to  $3.0 < \eta < 5.0$ , a separate forward calorimeter, HF, is introduced. For the HF, a modest hadron energy resolution ( $\sim 200\%/\sqrt{E} + 10\%$ ) along with a good jet identification capability is required. The good jet identification is needed to reject the fake jets formed by the particles coming from superimposed minimum biased events and for adequate tagging of jet angular resolution in the transverse plane.

The HF detector will consist of two modules, one on each end of the CMS detector. Each module is approximately 11 m from the interaction point (see figure 1).

The quartz fibre calorimeter technique has been studied and implemented by several groups [4–6]. There are several reasons that this particular quartz fibre (QF) design was selected for HF [7]. One of the main reasons is that HF will be operating in an extremely high radiation environment. At the pseudo-rapidity of  $\eta = 5$  and during the  $\sim 10$  years of operation, HF will experience  $\sim 1$  GRad of radiation. However, the quartz fibre calorimeter is intrinsically radiation hard [8]. Another reason is the insensitivity to low-energy neutrons since neutral particles do not generate Čerenkov light. At the HF location a high neutron flux will be present. A very fast response is another reason that this calorimeter technique was selected. At the LHC a bunch crossing will occur every 25 ns. Therefore, a calorimeter to operate in the LHC must be fast enough to accommodate this speed. This QF calorimeter technique was shown to be fast, producing a Čerenkov signal with a full width at half maximum of 3 ns [9].

In 1999, the HF collaboration built and tested the first pre-production prototype (PPP-I). The detector was placed on a platform that could move in three dimensions with respect to the H4 beam line of the Super Proton Synchrotron at CERN. The results presented in this note are on the spatial uniformity, electromagnetic and hadronic energy resolution and the energy response linearity of PPP-I. These results meet the design requirements of the CMS forward calorimeter mentioned above. The construction of this detector is now complete and ready to be installed at the CMS experimental collision hall at CERN.

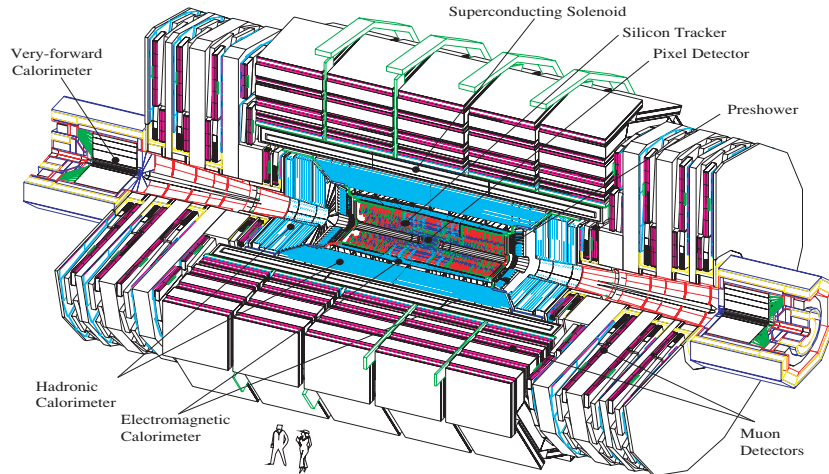


**Figure 1.** The CMS detector is shown. The different parts of the detector are marked as well as the forward calorimeter which is labelled as the very-forward calorimeter.

## 2. Pre-production-prototype I

The PPP-I is an iron absorber matrix with embedded quartz fibres which serve as the active material. The quartz core diameter of the fibre is  $300\ \mu\text{m}$  which is surrounded with a hard polymer (plastic) cladding of  $30\ \mu\text{m}$ . A  $50\ \mu\text{m}$  acrylate buffer covers the core and the cladding. The embedded fibres run parallel to the beam and constitute the active component of the detector. The iron matrix is composed of  $2.5\ \text{mm}$  thick iron layers with grooves every  $2.5\ \text{mm}$ . The length of the absorber is  $165\ \text{cm}$  ( $8.3\lambda_{\text{int}}$ ) with a cross sectional area of  $18\ \text{cm} \times 18\ \text{cm}$ . In each groove, a single quartz fibre is inserted. A total number of 6000 fibres are then grouped into 27 bundles. In PPP-I, there are three different lengths of fibres to achieve a longitudinal segmentation. They are called electromagnetic (EM),  $93.75\ X_0$ , hadronic (HAD),  $81.25\ X_0$ , and tail catcher (TC),  $17.05\ X_0$ . Long fibres sample all shower components while the shorter fibres are biased to the hadron component as the hadronic showers tend to penetrate deeper.

The physical spacing between fibres is the  $2.5\ \text{mm}$  groove spacing. The pattern used for the fibre insertion is shown in figure 2. There are two EM fibres for each HAD and TC fibre. The PPP-I is divided into nine physical regions called towers, each with a  $6\ \text{cm} \times 6\ \text{cm}$  cross sectional area (see figure 2). At the centre of each tower, a radioactive wire source-tube groove exists for calibration. Each fibre bundle (EM, HAD and TC) from a tower is coupled to a separate photomultiplier tube (PMT) via a light guide and read out as a separate ADC channel. The quartz fibres come off at the back of the  $1.65\ \text{m}$  long steel absorber and are bundled together to form the physical towers. Figure 3 shows a photograph of PPP-I before it was moved to the beam line.

## 3. Measurements

The data used in this analysis are summarized in table 1. For the calibration of the towers, a  $80\ \text{GeV}$  electron beam was directed at the centre of each tower. The gains of the photomultiplier tubes (PMT) were set such that the average of the nine towers' response to  $80\ \text{GeV}$  electrons was approximately 580 ADC channels above pedestal.

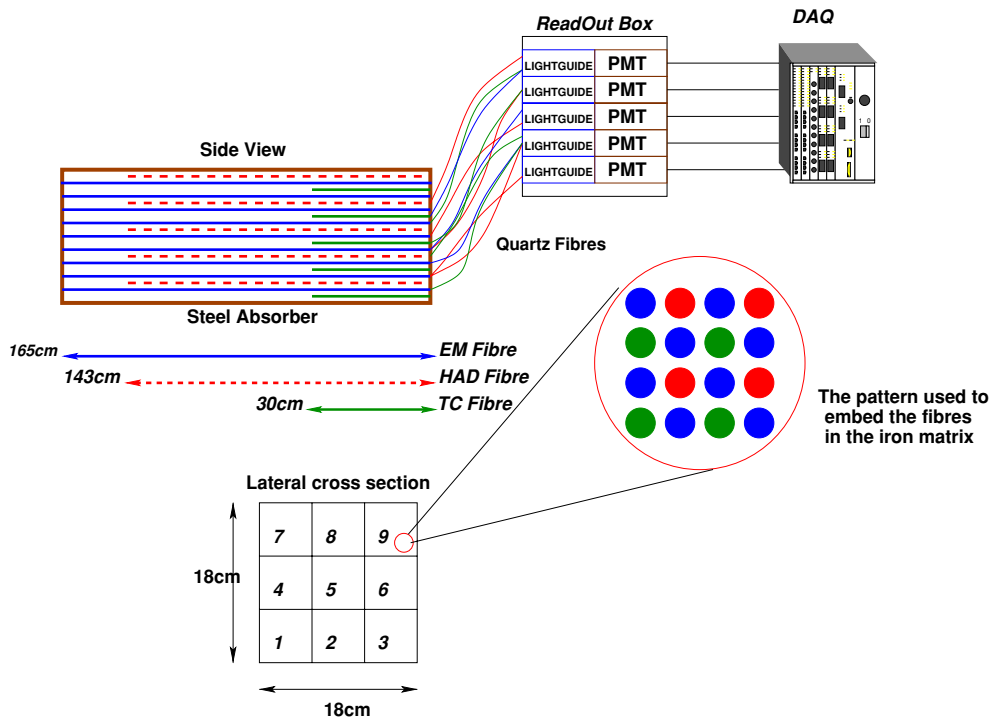


Figure 2. Schematic views of PPP-I.



Figure 3. PPP-I before it was moved to H4 beam line at CERN. The 1.65 m long iron absorber is seen on the right. The quartz fibres are also seen coming off the absorber and bundling at the iron ferrules.

However, the individual response of each tower could show variations. As an example of the typical response of a tower to electron beam, the signals recorded for a 100 GeV electron beam are shown in figure 4. The response of tower 5 to a 100 GeV electron beam is measured slightly higher (107.1 GeV).

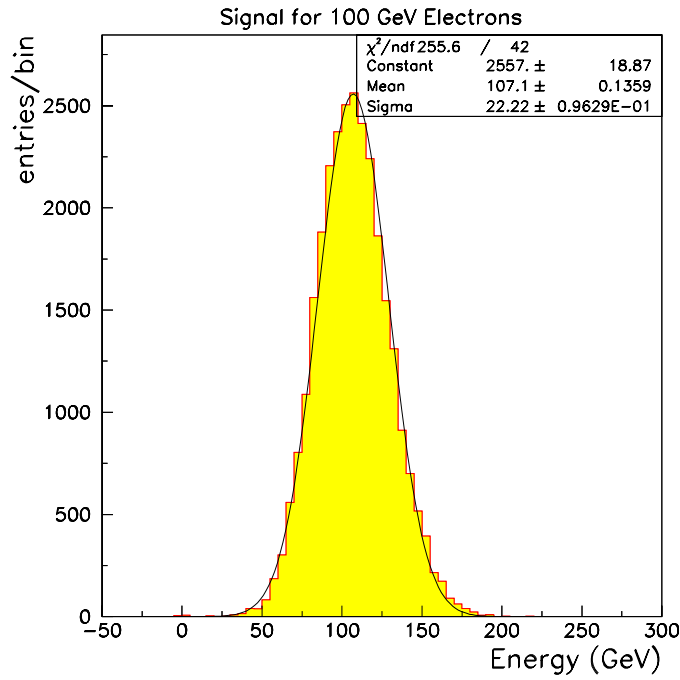


Figure 4. Tower 5 response of PPP-I to 100 GeV  $e^-$  s.

Table 1. Beam type and energies used for the analysis are listed.

Beam	Energy (GeV/ $c^2$ )
$e^-$	6, 8, 15, 20, 35, 50, 80, 100, 120, 150, 200
$\pi^-$	12, 15, 20, 35, 50, 80, 100, 120, 150, 175, 200, 225, 250, 275, 300, 350, 375

### 3.1. Spatial uniformity of PPP-I

One of the factors that affect the calorimeter's response is the non-uniformities in its structure. In PPP-I, this non-uniformity is the fibre spacing. When the beam particles enter the detector in an active layer, i.e. the quartz fibre, the sampling ratio is slightly higher than when they enter in the absorber. Particularly for electromagnetic showers, the shower is concentrated around its axis with a typical lateral dimension of the Molière radius ( $R_M$ ). For electromagnetic showers  $R_M$  is close to the radiation length  $X_0$  whereas for the hadronic showers, it is roughly half the size of the interaction length ( $\lambda_I$ ). It is also interesting to note that the lateral shower size is much less than that observed in  $dE/dx$  calorimeters [9]. So the detector response will have position-dependent variations. In PPP-I, these variations have periodic oscillations corresponding to the quartz fibre periodicity as shown below.

In order to study the spatial uniformity of the PPP-I, a 120 GeV electron beam was moved with 1.0 cm steps across the face of the detector and the signals of three adjacent towers (towers 4, 5 and 6. See figure 3) were plotted as a function of the beam position. The beam spot size was  $\sim 2 \text{ cm} \times 2 \text{ cm}$ . With the help of drift chambers located upstream, the impact position of every single particle of the beam on the detector face was known with a precision of 200  $\mu\text{m}$ .

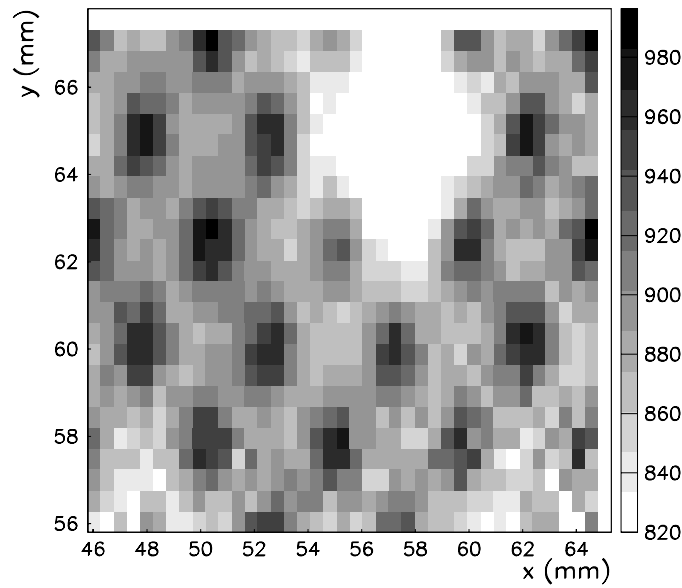


**Figure 5.** EM fibre locations revealed with 120 GeV electrons. The source-tube location is also visible. (See text for details.)

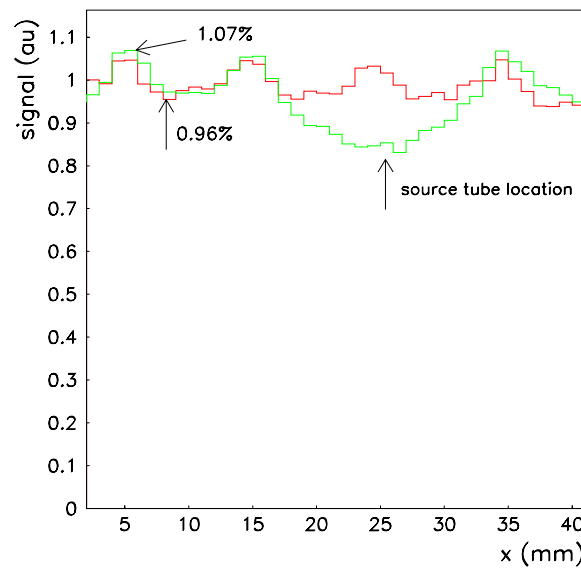


**Figure 6.** Overlaid  $x$ -projections of figure 5 at  $y = 60$  mm and  $y = 65$  mm.

Results of the beam scan are summarized in figures 5 and 6. As mentioned earlier, quartz fibres are embedded in the iron matrix as shown in figure 3. There are two EM fibres for each HAD and TC fibre giving rise to a 5 mm spacing between two EM fibres. This fibre periodicity can be seen in the beam scan data. The exact EM fibre locations are visible as dark spots in figure 5 which plots only the response of the EM fibres with a grey scale as a function of position. In the grey scale used, the darker colour corresponds to higher detector response

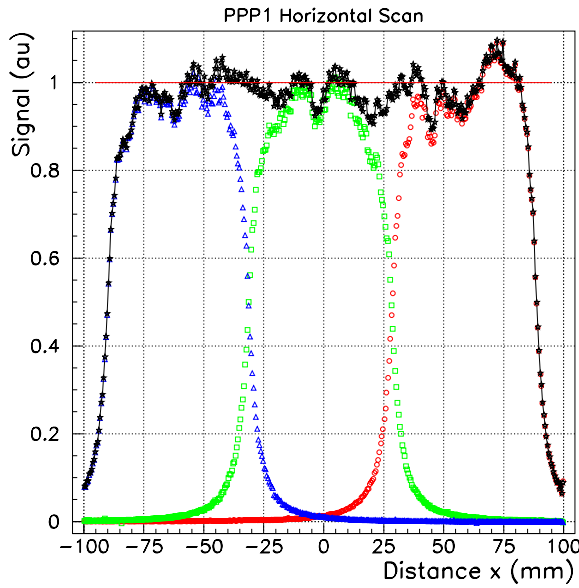


**Figure 7.** Horizontal scan along towers 4, 5, 6 (open triangles, squares and circles, respectively) with 120 GeV electrons and the sum of the signals of the three towers (stars connected with line).

and vice versa. The white coloured area between ( $64 \text{ mm} \leq y \leq 66 \text{ mm}$ ) and ( $54 \text{ mm} \leq x \leq 60 \text{ mm}$ ) in this figure corresponds to a source-tube groove that does not have a quartz fibre so as to allow the insertion of a radioactive wire source for calibration purposes.

Figure 6 shows the  $x$ -projection of the two-dimensional plot shown in figure 5 for two consecutive fibre layers. There is a  $\pm 6\%$  variation in the response of the detector due to the fibre periodicity. This is the result of the fact that the response of the calorimeter is slightly higher for particles entering the calorimeter in the fibre plane than for those entering in the absorber plane.

In figure 7, the response of the detector is shown for three adjacent towers (4, 5 and 6) as open triangles, squares and circles respectively. As the electron beam moves from one tower to another, the measured signal amplitudes for adjacent towers change. A sharp tower to tower transition is seen due to the narrow lateral profile of Čerenkov light generating particles. The sum of the signals of three towers is also shown in the same figure as stars with connected line.

A similar beam scan was also carried out with a 120 GeV  $\pi^-$  beam. The  $\pi^-$  beam was moved vertically across the face of the PPP-I. The signal amplitudes are shown in figure 8. Since the hadronic showers are not as narrow as electromagnetic ones, tower to tower transition profiles are not as sharp as in the electromagnetic case due to the larger tails. Therefore, the contribution of the adjacent towers to the total signal at a given tower position is higher compared to the scan made with electrons electromagnetic case (figure 8).

### 3.2. PPP-I energy resolution

The energy resolution of a calorimeter, in general, can be parametrized as

$$\left(\frac{\sigma}{E}\right)^2 = \left(\frac{a}{\sqrt{E}}\right)^2 + \left(\frac{b}{E}\right)^2 + c^2. \quad (1)$$

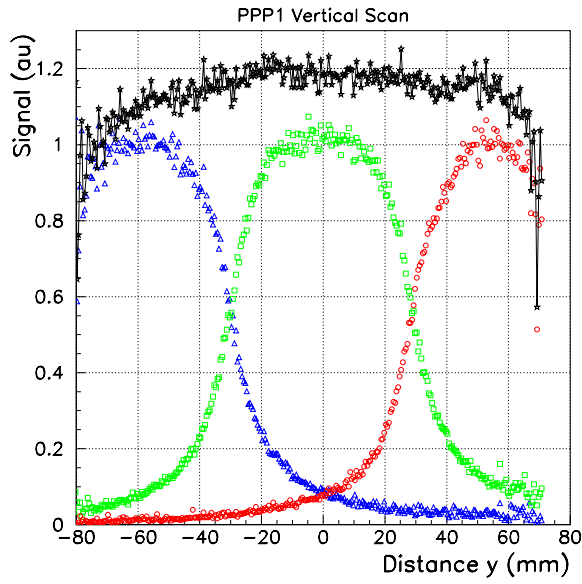


**Figure 8.** Vertical scan along towers 2, 5, 8 (open triangles, squares and circles, respectively) with 120 GeV pions and the sum of the signals of the three towers (stars connected with line).

The first term is the sampling term and characterizes the statistical fluctuations in the signal generating processes. The second term corresponds to noise and includes the energy equivalent of electronic noise as well as pileup. The third term is the constant term and is related to the imperfections of the calorimetry, signal generation and collection non-uniformity, calibration errors and fluctuations in the energy leakage from the calorimeter.

The energy resolution of PPP-I was studied in response to both electron and pion beams at different energies. The beam energies and the particle type used are summarized in table 1.

It had been shown in one of our earlier prototype tests [9–13] that in a quartz fibre calorimeter the electromagnetic energy resolution was completely dominated by photoelectron fluctuations. Therefore, when we characterize our electromagnetic energy resolution we can drop the noise term to give:

$$\left(\frac{\sigma}{E}\right)^2 = \left(\frac{a}{\sqrt{E}}\right)^2 + c^2. \quad (2)$$

The response of the PPP-I has been recorded as a function of beam energy. The calorimeter's response to electrons is seen to be Gaussian. However, a deviation from Gaussian behaviour is seen in the response to the  $\pi^-$  beam. This is a result of the different natures of electromagnetic and hadronic showers [14]. Another point that should be noted here is the fact that the response of the detector is lower for pions than for electrons, as seen in figures 4 and 9.

This is a characteristic of the quartz fibre Čerenkov detectors because of the fact that the hadronic showers register in the detector only through their electromagnetic components. The part of the hadronic showers that is not converted into electromagnetic ones through  $\pi^0$  production goes unregistered and hence the Čerenkov process gives rise to a lower response which also implies  $e/h > 1$ . This phenomenon is also the reason for the nonlinear behaviour

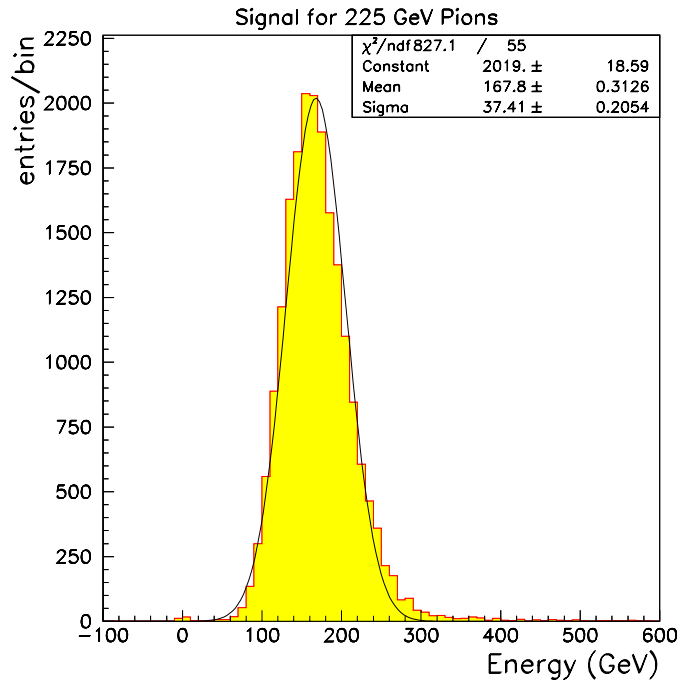


Figure 9. Tower 5 response of PPP-I to 225 GeV  $\pi^-$  s.

of this detector to hadrons. At low energies, the fluctuations of the electromagnetic component of the hadronic showers are larger.

Of the secondary hadronic particles, mostly  $\pi^0$ s contribute to the Čerenkov signal since they decay into two photons which in turn contribute to the electromagnetic core and register in the detector as Čerenkov light. Other non-electromagnetic secondaries are mostly not relativistic and therefore do not give rise to Čerenkov light and hence do not register in the detector. At low energies, the number of  $\pi^0$ s in the shower is characterized by a Poisson distribution which becomes more and more Gaussian at high energies.

Figure 10 shows the energy resolution for electrons as a function of energy. The resolution ( $\sigma/E$ ) is plotted against  $1/\sqrt{E}$  and fitted to equation (1). The fit yields

$$\left(\frac{\sigma}{E}\right)^2 = \left(\frac{197\%}{\sqrt{E}}\right)^2 + (8\%)^2.$$

Hadronic energy resolution of PPP-I as a function of energy is shown in figure 11. At 1 TeV, the energy resolution is below 20%.

### 3.3. Energy response linearity

PPP-I exhibits a different response to electromagnetic and hadronic showers. The data sample used in this study is shown in table 1. The response of the PPP-I was recorded as a function of beam energy.

The measured response to electrons (figure 12) was normalized by dividing by the beam energy and the response to 35 GeV and plotted against the beam energy. The response to pions was normalized by the beam energy and plotted against the beam energy as shown in figure 13.

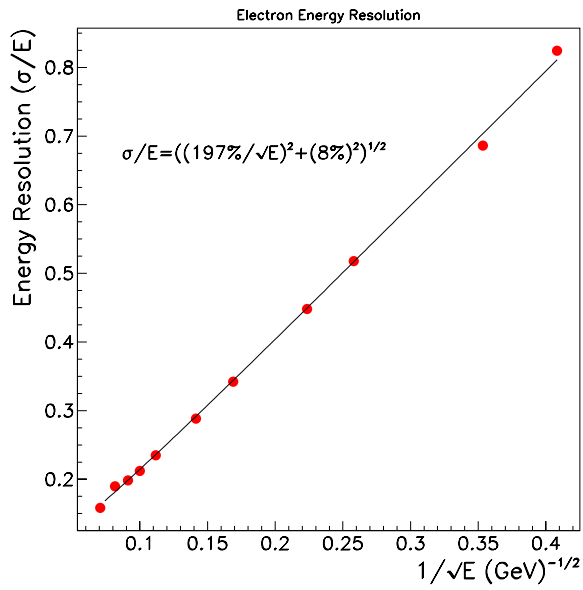


Figure 10. Electromagnetic energy resolution as a function of  $1/\sqrt{E}$ .

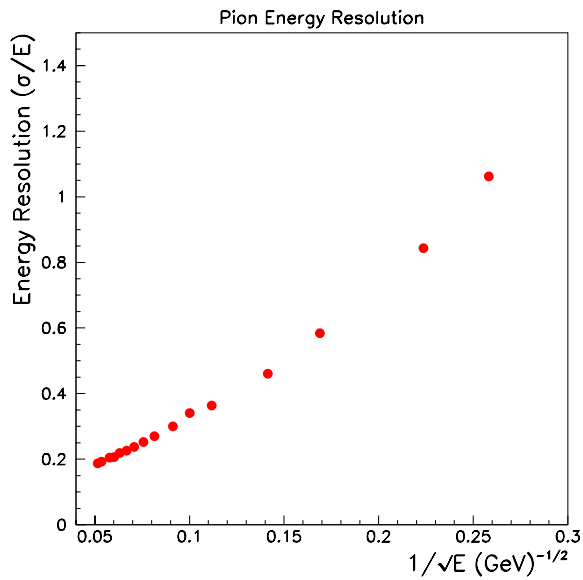
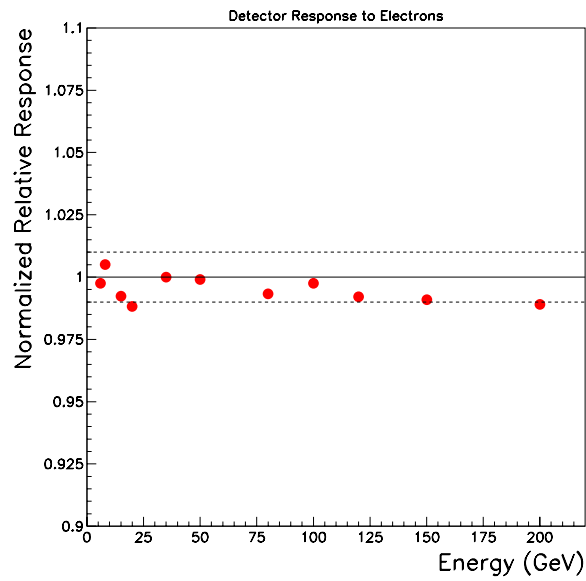
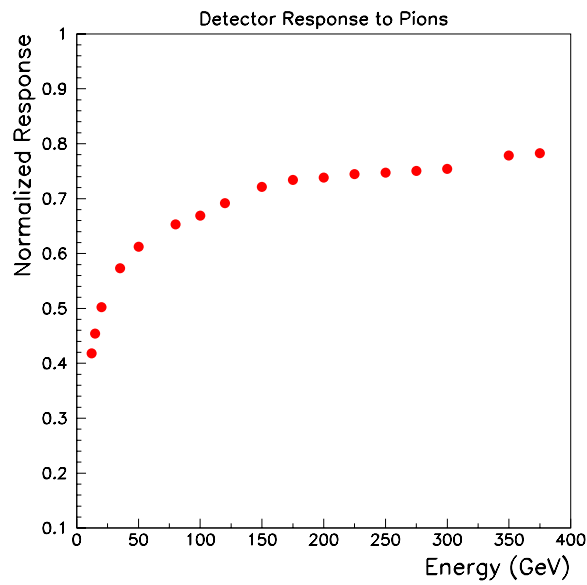


Figure 11. Hadronic energy resolution as a function of  $1/\sqrt{E}$ .

The response as a function of electron beam energy is linear to within 1%. However, as seen in figure 13, the response as a function of energy is nonlinear for hadronic beams. This is due to the electromagnetic portion of the hadronic shower, that is, the  $\pi^0$  content. As the beam energy increases, the  $\pi^0$  fraction increases giving rise to a larger Čerenkov signal in the detector.



**Figure 12.** Normalized relative (to the response to 35 GeV) response to  $e^-$  s as a function of beam energy.



**Figure 13.** Normalized response to  $\pi^-$  s as a function of beam energy.

#### 4. Summary and conclusions

A pre-production-prototype for the forward calorimeter of the CMS detector has been tested at the H4 beam line at CERN. The electromagnetic energy resolution was measured to be  $\left(\frac{\sigma}{E}\right)^2 = \left(\frac{197\%}{\sqrt{E}}\right)^2 + (8\%)^2$ . The hadronic energy resolution was determined to be 20% at 1 TeV.

The response was found to be linear to 1% for electrons. A highly nonlinear behaviour for hadrons was observed.

### Acknowledgments

We would like to thank our colleagues from CMS in particular J Bourotte and M Haguenaer for their assistance in the various tests described in this note. We also thank Jim Freeman, Dan Green, Andris Skuja, Aldo Penzo and Jim Virdee from CMS for their encouragement and support. This work was supported by the US Department of Energy (DE-FG02-91ER-40664) and NSF (NSF-JNT-98-20258), the Hungarian National Fund (OTKA T026184), the International Science Foundation (grants M 82000 and M 82300), the State Committee of the Russian Federation for Science and Technologies, and the Russian Research Foundation (grant 95-02-04815) and the Scientific and Technical Research Council of Turkey (TUBITAK).

### References

- [1] CMS Collaboration 1994 *Technical Proposal* CERN/LHCC 94-39
- [2] CMS Collaboration 1997 *The Electromagnetic Calorimeter Project Technical Design Report* CERN/LHCC 97-33
- [3] CMS Collaboration 1997 *The Hadron Calorimeter Project Technical Design Report* CERN/LHCC 97-31
- [4] Anzivino G *et al* 1995 *Nucl. Instrum. Methods A* **357** 369
- [5] Gorodetzky P *et al* 1995 *Nucl. Instrum. Methods A* **361** 161
- [6] Adler C *et al* 2001 *Nucl. Instrum. Methods A* **470** 488
- [7] Onel Y 2002 Invited talk at *10th Int. Conf. on Calorimetry in High Energy Physics, CALOR 02 (CalTech, CA, 25–29 March 2002)* ed R Y Zhu (Singapore: World Scientific) pp 504–20
- [8] Dumanoglu I *et al* 2002 *Nucl. Instrum. Methods A* **490** 444
- [9] Akchurin N *et al* 1997 *Nucl. Instrum. Methods A* **399** 202
- [10] Akchurin N *et al* 1998 *Nucl. Instrum. Methods A* **409** 593
- [11] Akchurin N *et al* 1998 *Nucl. Instrum. Methods A* **408** 380
- [12] Akchurin N *et al* 1997 *Nucl. Instrum. Methods A* **400** 267
- [13] Akchurin N *et al* 1996 *Nucl. Instrum. Methods A* **379** 526
- [14] Wigmans R 2000 *Calorimetry: Energy Measurement In Particle Physics* (Oxford: Oxford University Press)